INTERNATIONAL JOURNAL of RENEWABLE ENERGY RESEARCH
P. Irasari et al., Vol.16, No.1, March, 2026

A Comparative Study of Performance and Manufacturing Costs between Axial and Radial Flux Permanent Magnet Generators Considering Permanent Magnet Shape

Pudji Irasari*, Ketut Wirtayasa*, Puji Widiyanto*, Muhammad Kasim*‡

*Research Centre for Energy Conversion Technology, National Research and Innovation Agency, Jl. Raya Puspiptek 60, Tangerang Selatan 15310, Indonesia

(pudj003@brin.go.id, ketu003@brin.go.id, puji010@brin.go.id, muha087@brin.go.id)

‡Corresponding Author; Muhammad Kasim, Jl. Raya Puspiptek 60, Tangerang Selatan 15310, Indonesia,

Tel: +62 821 2541 7705, muha087@brin.go.id

Received: 11.01.2024 Accepted:09.02.2024

Abstract- This study compares the performance and cost aspects of two types of machines: axial flux permanent magnet generators (AFPMG) and radial flux permanent magnet generators (RFPMG). Four machine topologies, each generating 600 W at 835 rpm, are analysed, including single-gap AFPMGs with rectangular (RTG) and trapezoidal (TPZ) permanent magnet rotors, as well as single-gap inner rotor RFPMGs with curved (CRV) and RTG permanent magnet rotors. Parameters such as the pole arc coefficient, stator slot dimensions, stator yoke, and magnet volume are constant across all topologies. Simulation using Ansys Maxwell 3D is employed to evaluate the performance of these machines, comparing magnetic flux distribution, air gap flux density, output power, and output torque. Furthermore, a comprehensive cost analysis is conducted based on the price of the weight of the active materials and the price from the local workshop. Results indicate that the RTG AFPMG exhibits the highest output power and power-to-weight ratio. Additionally, it demonstrates the lowest manufacturing cost and cost per power unit ratio compared to other topologies. Therefore, based on technical and economic considerations, this study concludes that the AFPMG with rectangular magnets offers the most favourable choice for practical applications.

Keywords Single-side AFPMG, single-gap internal rotor RFPMG, ansys maxwell 3D, performance analysis, cost analysis.

1. Introduction

The increasing global energy demand and growing environmental concerns have prompted energy suppliers to prioritize energy sustainability by increasing the utilization of renewable energy sources such as solar, wind, hydro, and ocean. Extensive research identifies that a permanent magnet generator (PMG) is a highly suitable technology for small-scale wind and hydropower, particularly in rural and urban areas, owing to its numerous advantages [1] [2] [3] [4] [5] [6].

The axial flux permanent magnet generator (AFPMG) and the radial flux permanent magnet generator (RFPMG) have emerged as two widely adopted types of machines. Consequently, many studies have comprehensively analysed the two machines separately or compared their performance and economic feasibility. Studies on AFPMG and RFPMG have been found many for small-scale wind and hydro applications, with capacities up to 5 kW. The research about PMG with axial flux type in wind turbines can be located within the references [7] [8] [9] [10] [11] [12] [13] [14], whereas the investigation on Pico hydro is documented in [2] [15] [16] [17]. Meanwhile, the discourse regarding the radial flux type for wind turbines is expounded upon by [18] [19] [20] [21], while [22] [23] [24] [25] addresses the discussion on Pico hydro.

Even though AFPMG and RFPMG demonstrate numerous applications in small-scale hydro energy, the focus of comparative studies primarily lies within their implementation in wind turbine applications. Notable research conducted by [26] [27] [28] [29] [30] [31] further delves into this domain. Reference [26] compares the performance and manufacturing costs of the 550 W AFPMSG and RFPMSG based on 3D modelling. The axial flux machine has nearly half the volume of the radial flux machine and boasts a superior torque-to-weight ratio so that it can be more cost-effective owing to reduced material consumption. In reference [27], a 3 kW conventional RFPMG and a double-sided coreless AFPMG are compared. The evaluation considers losses, output power, total harmonic distortion (THD), frequency, and induced electromotive force (emf). In addition, ANSYS Maxwell software and the finite element method are used to examine the AFPMG's performance. The results conclusively show that the AFPMG outperformed the RFPMG in all studied areas. Furthermore, reference [28] examines the operation of permanent magnet wind turbines while explicitly considering the magnetic flux directions during mechanical energy storage. Each generator's electromagnetic properties, such as voltage, losses, output power, and efficiency, are examined using measured current, accounting for harmonic influences. Experiments are used to evaluate performance, and the results show that, given similar electrical conditions, the RFPMG performs somewhat better than the AFPMG.

The study by reference [29] examined the efficiency and cost-effectiveness of different 3 kW machine topologies. The study considered active materials such as copper wire, iron core, permanent magnets, and shaft. Manufacturing costs were estimated using a cost factor of 1.5 for double-rotor single-stator AFPMG and 2.0 for inner and outer rotor RFPMGs, respectively. The results indicated that AFPMG and inner RFPMG had slightly higher efficiency. Furthermore, despite having greater active material prices than outer and inner rotor RFPMG, AFPMG's total anticipated costs were lower. It was primarily related to lower manufacturing costs at AFPMG.

Reference [30] focuses on the cost investigation of two ferrites PMG topologies: double-sided inner-stator AFPMG and spoke-type RFPMG. The analysis considers the costs of active materials (copper, permanent magnets, iron) and manufacturing (with a manufacturing coefficient of 1.5 for AFPMG and 2 for RFPMG). AFPMG incurs higher costs due to twin rotor permanent magnets. Nevertheless, finite element computation results show that both topologies are ideal for low-speed micro-wind power applications.

In reference [31], a comparison is made between the slotted AFPMG and RFPMG. Both machine types are optimized through computer-based design modelling to achieve the lowest cost/torque ratio. Additionally, design optimization for maximum torque/volume is explored. The calculations demonstrate that the two machines' efficiency is quite comparable, and the RFPMG exhibits lower cost/torque than the slotted AFPMG and lower torque/volume.

Based on the literature study above, this paper provides an extensive performance and cost analysis comparison between small-scale AFPMG and RFPMG types. Four machine topologies are analysed, and each machine generates an output power of 600 watts at an operating speed of 835 rpm. The machines are single gap internal rotor RFPMG with curved and rectangular magnets and single-side AFPMG with trapezoidal and rectangular magnets. Some parameters with the same value for all machine topologies are pole arc coefficient, stator slot dimension, stator yoke, and magnet volume. To find the machine characteristics, the 3D Ansys Maxwell is used for the FE analysis. The characteristics that will be compared include the magnetic flux distribution, air gap flux density, output power, and output torque. Manufacturing costs are calculated using the price of active material weight approach compared to local workshop prices. The latest is intended to probe the effect of magnet shapes on the cost of the manufacturing process.

2. Modelling of the Generators

The generator modeling focuses on geometric considerations, specifically the determination of the shape, arrangement, and dimensions of its components, including the stator, rotor, and permanent magnets. Fig. 1 illustrates the studied shapes and arrangements of the generator components, with AFPGM depicted in Fig. 1(a) and RFPMG in Fig. 1(b), while detailed dimensions are provided in Table 1. Following this, the next step involves determining the material properties.

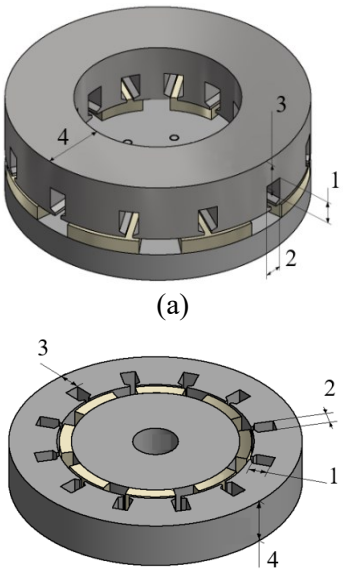

Description: 1. Stator slot height, 2.Stator slot width, 3. Stator yoke height, 4. Stator core length

Fig. 1. Generator topology with several parts having the same dimensions are indicated by the same number, (a) single-side AFPMG and (b) internal rotor RFPMG.

The generator is excited with eight permanent magnet poles, and the stator windings are accommodated in 12 stator slots. The permanent magnet used in this design is N35SH with a residual magnetic flux density (B_r) of 1.17 T, a coercivity field strength (H_{cB}) of 876 kA/m, its axial height

(h_m) of 10 mm, and glued on the surface of the rotor core. The stator material is JFE steel 50JN470 lamination with a maximum flux density of 2.4173 T (Fig. 2), while the rotor uses carbon steel. In the design, the flux density is restricted to a maximum value of 2 T to prevent saturation.

Table 1. Stator and rotor dimensions

No.	Parameters	AFPM	RFPM	Unit
Stator				
1	Outer diameter	190	244	mm
2	Inner diameter	110	164	mm
3	Core length	40		mm
4	Slot height	16		mm
5	Slot width	13		mm
6	Yoke height	20		mm
Rotor				
7	Outer diameter	190	140	mm
8	Inner diameter	110	47	mm

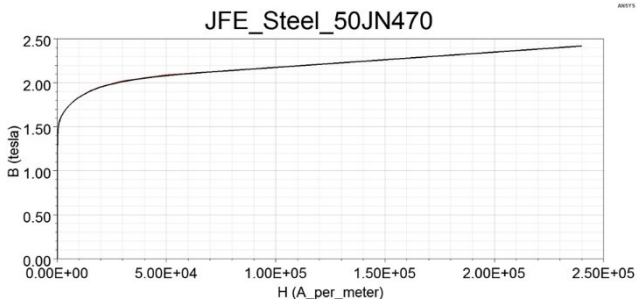

Fig. 2. The B – H curve of JFE Steel 50JN470 taken from Ansys Maxwell software.

Certain limitations exist in determining machine dimensions, including magnet volume uniformity. Additionally, various parameters such as stator slot and tooth sizes, stator yoke height, core axial length, winding count, wire and shaft diameters remain constant between both machines. The pole width-to-pole pitch ratio, denoted as α_i, is fixed at 0.68.

This study analyses two magnet shapes for AFPMG (trapezoidal and rectangular) and two for RFPMG (curved and rectangular). By maintaining the specified values of α_i and volume, the rectangular AFPMG magnet matches the curved magnet's surface area, and the rectangular RFPMG magnet nearly matches the trapezoidal one. These four magnet shapes define the research limitation, with detailed dimensions shown in Fig. 3: (a) trapezoidal (TPZ) AFPMG magnet, (b) rectangular (RTG) AFPMG magnet, (c) curved (CRV) RFPMG magnet, and (d) RTG RFPMG magnet.

To achieve the same surface area and volume with RFPMG, the thickness of the rectangular magnet shape for AFPMG should be adjusted to 9.4 mm. The per-phase winding arrangement for the AFPMG and RFPMG with star configuration is shown in Fig. 4, with AFPMG in Fig. 4(a) and RFPMG in Fig. 4(b). The generators are equipped with the non-overlap fractional slot winding type considering several advantages as discussed in [32, 33].

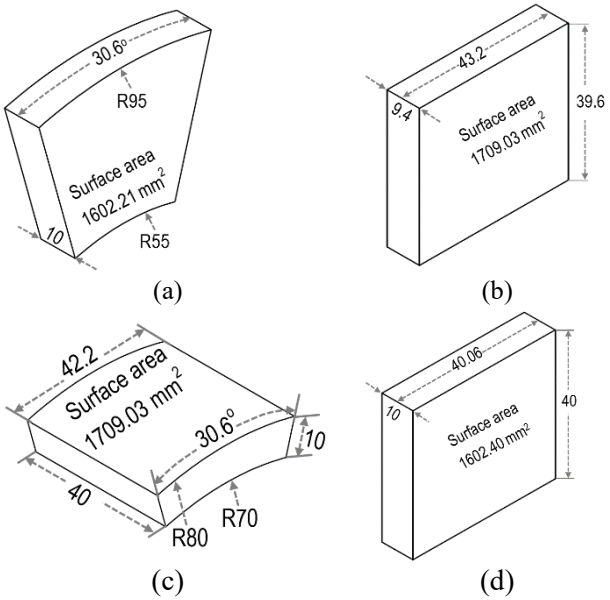

Fig. 3. Magnet shapes and dimensions in mm unit (a) TPZ magnet, (b) RTG magnet for the AFPMG, (c) CRV magnet, and (d) RTG magnet for the RFPMG.

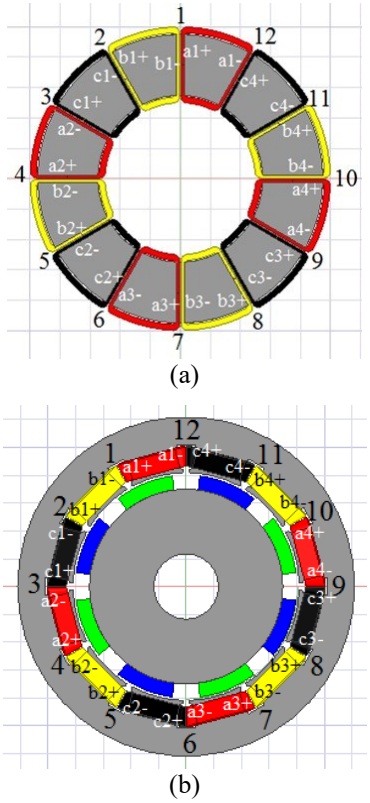

Fig. 4. Winding arrangement per phase based on the star of slot approach. (a) single-side AFPMG, (b) internal rotor RFPMG.

3. Performance Simulation

The machine performances and characteristics such as back EMF, armature current, output power, output torque and efficiency, are obtained through the finite element analysis simulation from the Ansys Maxwell software. In numerical analysis, the back EMF of the machine is the direct product of the stator winding conductor length, the flux density vector, and the machine speed [34, 35]:

$$E = \oint (\vec{v} \, x \, \vec{B}) \, dl \quad (1)$$

where E represents the induced EMF in the stator winding, B refers to the air gap flux density, and v is the conductor's linear velocity. This equation can be detailed further to the equation for the phase EMF [35]:

$$E_{ph} = \frac{\sqrt{2}}{2} B_g \omega_m k_w N_{ph} D_{av} L_i \; (2) \quad (2)$$

where ω_m is the mechanical speed, k_w is the winding factor, N_{ph} refers to the number of turns per phase, and L_i is the conductor length. At the condition when the loads are connected, the phase voltage is expressed in phasor form as [35]:

$$V_t = E - \Delta V \quad (3)$$

$$= E - i\,((R_s + jX_s) + R_L) \quad (4)$$

where V_t is the terminal voltage, ΔV is the voltage drop, R_s refers to machine resistance, X_s refers to machine reactance, and R_L is the connected load. The output power (P_o) of the machine can be estimated as the product of phase voltage and phase current:

$$P_o = 3 \text{ x } V_t \text{ x } i \text{ x } \cos\theta \quad (5)$$

The torque can be calculated using the relation of the power input P_i and the angular speed of the motor as shown as follows [35}:

$$T = \frac{P_i}{\omega} \quad (6)$$

$$T = \frac{P_i}{2\pi \frac{n}{60}} \quad (7)$$

where T represents the torque, r represents the radius, ω represents the angular speed, and n represents the rotational speed.

The efficiency can be obtained with

$$\eta = \frac{P_o}{P_i} \times 100\% \quad (8)$$

4. The Active Components of the Machine

The determination of manufacturing process costs is contingent upon the active components of the machine, encompassing the stator, rotor, windings, and permanent magnets, as delineated in Table 2, in conjunction with the pertinent material specifications. Manufacturing expenditures, predicated upon the weight of active materials, are subject to utilization coefficients of 1.5 for AFPMG and 2 for RFPMG . The outcome will be juxtaposed with the manufacturing cost prevailing at the local workshop, facilitating a comprehensive comparative assessment.

Table 2. The specification of the active components

No.	Components	Specifications
1	Rotor	Carbon steel, ST-37
2	Stator	Silicon Steel sheet
3	Magnet	NdFeB grade 35SH
4	Winding	Copper wire

5. Results and Discussion

5.1. Magnetic Characteristics

Fig. 5 illustrates the three-dimensional magnetic flux density distribution in the machine's model at nominal load. The visualization indicates that the machine does not exhibit any magnetic flux concentration exceeding 2 T (see Fig. 2), indicating the absence of magnetic saturation. It is mainly observed in the stator teeth and along the air gap.

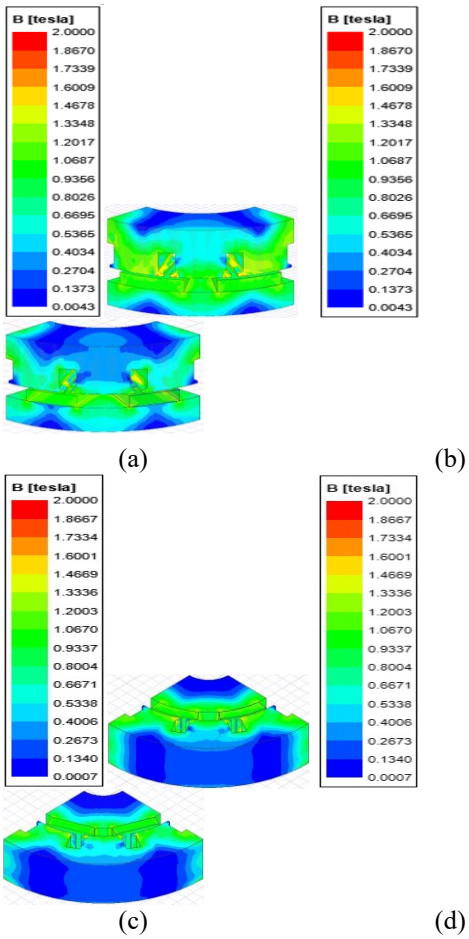

Fig. 5. Magnetic field distribution based on simulation result for (a) trapezoidal magnet AFPMG, (b) rectangular magnet AFPMG, (c) CRV RFPMG, and (d) RTG RFPMG.

The simulation results reveal specific disparities in the magnetic flux distribution. Notably, the AFPMG with a trapezoidal magnet shape, depicted in Fig. 5(a), demonstrates

a greater concentration of flux density around the stator teeth compared to the surrounding regions, including the stator core and air gap.

The second configuration, AFPMG with a rectangular magnet shape, depicted in Fig. 5(b), exhibits a lower concentration of flux density in the stator teeth and air gap compared to the trapezoidal shape. This reduced concentration is attributed to the larger effective area of the air gap—the broader gap between magnets in this configuration results in increased flux leakage and fringing flux. Consequently, a smaller magnetic flux density accumulates in the stator teeth and air gap, leading to a lower effective magnetic flux density.

The magnetic flux density distribution exhibits a heightened emphasis on the stator teeth and air gap in the case of the third configuration, namely RFPMG with a curved magnet shape, as visually represented in Fig. 5(c). This distribution pattern resembles the trapezoidal magnet shape but shows a diminished concentration along the stator yoke. Such a phenomenon signifies a reduced magnitude of flux traversing through the stator yoke.

Lastly, the RFPMG with a rectangular magnet portrayed in Fig. 5(d) vividly illustrates that the magnetic flux density distribution within the stator teeth and yoke is comparatively more minor when compared to the other topologies. This disparity arises due to the variable and asymmetrical effective air gap distance between the stator and rotor. Consequently, the magnetic flux encounters impediments in achieving uniform dispersion, resulting in a less pronounced concentration within the teeth and stator yoke.

Fig. 6 shows the magnetic flux density (B_δ) waveform (Fig. (6(a)) and back EMF (Fig. 6(b)). It can be seen that all four machine topologies have similar shapes. The peak value of the B_δ for each topology are 1.077 T for TPZ magnet AFPMG, 0.986 T for RTG magnet AFPMG, 1.011 T for CRV magnet RFPMG, and 0.859 T for RTG RFPMG.

While all machine topologies have the same number of turns, the TPZ AFPMG produces the highest B_δ. However, the RTG AFPMG exhibits the highest linkage flux at 0.0806 Wb due to its superior rotor-to-stator pole area ratio of 0.725, compared to 0.680 for TPZ AFPMG and 0.0663 for CRV RFPMG. Notably, all machines have identical air gaps. The use of rectangular magnets in RFPMG leads to a wider air gap in the magnet's middle section, resulting in a smaller B_δ amplitude and a reduced rotor-to-stator pole area ratio of 0.662, resulting in the lowest linkage flux of 0.0649 Wb among the four topologies.

For back EMF, all machine topologies exhibit a similar waveform. RTG AFPMG achieves the highest back EMF at 20.01 V, surpassing CRV RFPMG (18.93 V), TPZ AFPMG (18.43 V), and RTG RFPMG (15.95 V). RTG AFPMG also demonstrates the smoothest waveform, indicating the lowest Total Harmonic Distortion (THD) at 14.5%, implying minimal waveform distortion.

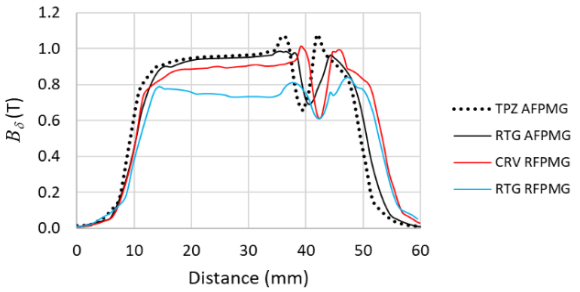

(a)

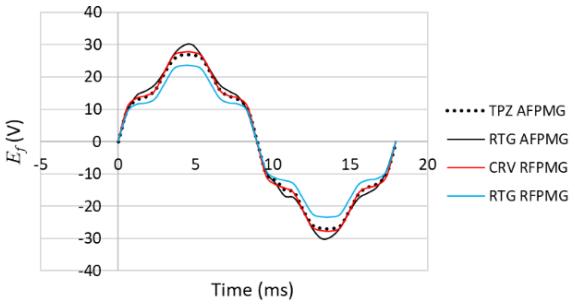

(b)

Fig. 6. Magnetic characteristics, (a) no load air gap magnetic flux density B_δ and (b) back EMF.

5.2. Electrical Parameters

Table 3 details stator winding calculations, including turn count, wire specifications, resistance, and inductance. The primary winding parameters (turns and diameter) are assumed to be identical. Notably, the radial topology has longer end turns and coil tracks, resulting in more considerable per-phase winding length and volume, consequently leading to higher phase resistance.

Table 3. Stator winding data

No.	Parameters, unit	AFPMG		RFPMG	
		TPZ	RTG	CRV	RTG
1	Phase winding numbers, *turns*	64			
2	Wire diameter, *mm*	1.96			
3	Winding length per phase, *m*	9		11	
4	Winding volume, *kg*	0.73		0.89	
5	Resistance, Ω	0.07		0.08	
6	Synchronous inductance, *mH*	0.293	0.322	0.299	0.291

Regarding inductance, Maxwell simulations yield synchronous inductance, which encompasses mutual and leakage inductance. Mutual inductance is flux-linkage dependent, while leakage inductance remains constant. Consequently, RTG AFPMG exhibits the highest synchronous inductance due to its superior linkage flux.

Under a 1.5-ohm resistive load per phase during simulation, results depicted in Fig. 7 reveal proportional relationships between flux linkage, output power P_o, (Fig. 7(a)) and torque T (Fig. 7(b)). RTG AFPMG with the highest flux linkage outperforms other topologies in P_o, and T, followed by CRV RFPMG, TPZ AFPMG, and RTG RFPMG, respectively.

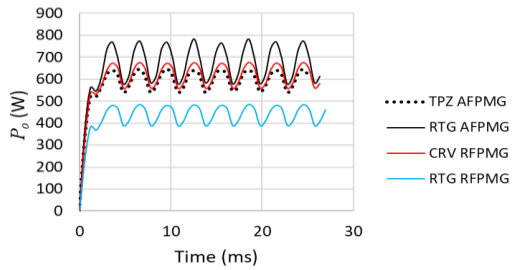

(a)

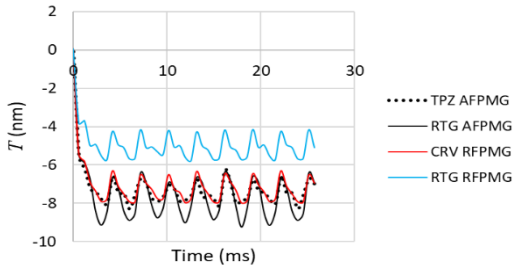

(b)

Fig. 7. The simulation results for load condition for (a) output power and (b) torque.

The other electrical parameters of the machine in load condition (in rms value) are presented in Table 4. It can be seen that the AFPMG has higher value in machine parameters compared with the RFPMG. In more detail, the RTG AFPMG shows the highest value in all parameters, while RTG RFPMG has the lowest value.

5.3. Manufacturing Cost

This study calculates manufacturing costs for active components, with stator and rotor parts made using laser cutting technology. Rotor shapes with and without magnet permanen for TPZ and RTG AFPMG are shown in Fig. 8(a) & 8(b), while CRV and RTG RFPMG are in Fig. 8(c) & 8(d). AFPMG has larger rotor dimensions, requiring more material, and Fig. 8(d) displays a permanent magnet base for rectangular magnets.

In RFPMG, the stator core is laser-cut to create stacked laminations for a 40 mm thickness (Fig. 9(a)). In contrast, for AFPMG, the stator is made by cutting and rolling the material to achieve a 40 mm thickness (Fig. 9(b)). The weights of the active components for each generator are detailed in Table 5.

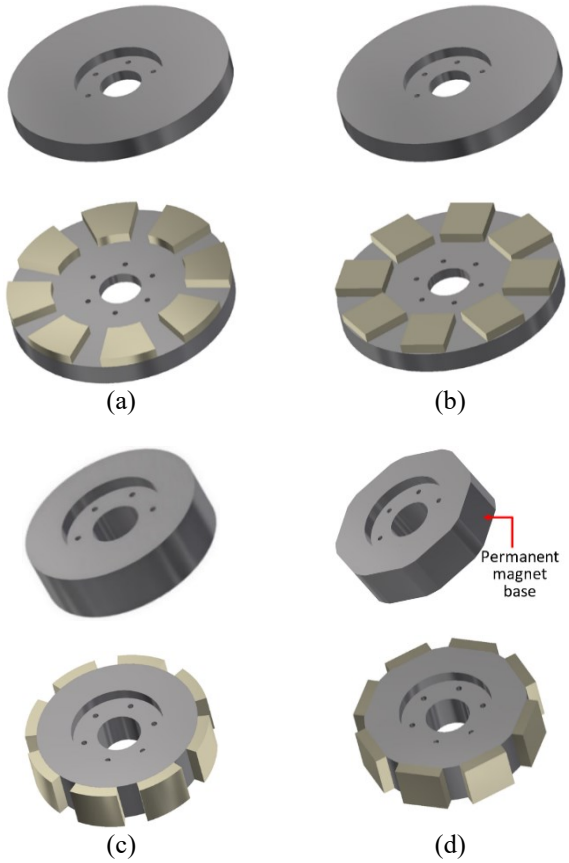

(a) (b) (c) (d)

Fig. 8. Rotor with and without magnet permanent for (a) TPZ AFPMG, (b) RTG AFPMG (c) CRV RFPMG, and (d) RTG RFPMG.

Table 4. Generator parameters in load condition

No.	Parameters, symbol	AFPMG		RFPMG		Unit
		TPZ	RTG	CRV	RTG	
1	Phase current, I_a	11.72	12.50	11.95	9.91	A_{rms}
2	Phase terminal voltage, V_t	17.57	18.75	17.92	14.87	V_{rms}
3	Input power, P	633.26	719.26	662.63	474.70	W
4	Output power, P_o	593.68	674.68	618.05	442.03	W
5	Torque, T	7.46	7.86	7.32	5.11	Nm
6	Efficiency, η	93.75	93.80	93.27	93.12	%

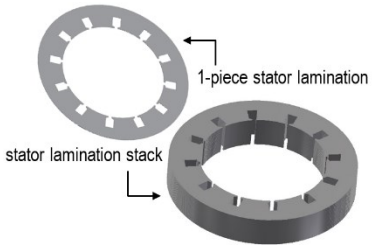

(a)

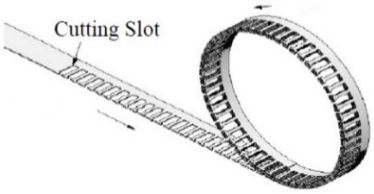

(b)

Fig. 9. Stator cutting results with laser cutting for (a) RFPMG and (b) AFPMG. [36]

Table 5. Weight of active components for each generator

Part num.	Part name	Weight (kg)			
		AFPMG		RFPMG	
		TPZ	RTG	CRV	RTG
1	Rotor	4.46	4.46	4.15	3.95
2	Stator	5.91	5.91	7.16	7.16
3	Magnet	0.99	0.99	0.99	0.99
4	Winding	0.73	0.73	0.89	0.89
Total weight		12.07	12.07	13.17	12.97

The generators' power-to-weight ratios are as follows, from highest to lowest: RTG AFPMG (55.90 W/kg), TPZ AFPMG (49.19 W/kg), CRV RFPMG (46.93 W/kg), and RTG RFPMG (34.08 W/kg).

Active material costs are based on prices per kg: silicon steel sheet (IDR 50,000/kg), winding (IDR 240,000/kg), and permanent magnet (IDR 1,915,313/kg, converted from USD 123 at an exchange rate of 1 USD = 15,571.65 IDR [37]). See Table 6 for detailed active material prices and manufacturing costs.

Table 6 shows that manufacturing costs for AFPMG variants consistently outperform RFPMG, with an average 27% reduction. A comparison is made to local workshop expenses in Table 7. The permanent magnet cost is given in Chinese Yuan and converted to Indonesian Rupiah (IDR) at 1 Yuan = 2,172.26 IDR. These tables reveal that permanent magnets are the most expensive among active components. Based on uniform weights, magnet prices in Table 6 are lower than supplier rates in Table 7, with an average difference of 76.88%.

Table 6 shows CRV RFPMG rotor cost exceeds RTG RFPMG, but Table 7 reveals the reverse from workshop-derived manufacturing costs. In both tables, CRV RFPMG consistently costs more than RTG RFPMG.

CRV RFPMG's lower manufacturing cost in Table 7 is due to its smaller size, processed using a lathe machine. RTG RFPMG, needing a milling process for magnet installation (Fig. 8(d)), incurs higher costs. For AFPMG stators, higher manufacturing costs result from making jigs for sheet rolling.

The substantial manufacturing cost disparity between Table 7 and Table 6 likely arises from Table 7's cost estimation predicated on single-component fabrication, whereas machine settings and jigs enable mass production. Therefore, the manufacturing costs presented in Table 6 are considered to align more favourably with mass production, while those in Table 7 pertain solely to one-unit production.

Table 6. Manufacturing cost based on active material weight

Part num.	Active materials	Cost (IDR)			
		AFPMG		RFPMG	
		TPZ	RTG	CRV	RTG
1	Rotor	223,000	223,000	207,500	197,500
2	Stator	295,500	295,500	358,000	358,000
3	Magnet	1,857,854	1,857,854	1,857,854	1,857,854
4	Winding	175,200	175,200	213,600	213,600
Total active material cost		2,551,554	2,551,554	2,636,954	2,626,954
Manufacturing coeff.		1.5	1.5	2	2
Manufacturing cost		3,827,331	3,827,331	5,273,908	5,253,908

Table 7. Manufacturing cost at the local workshop

No.	Active materials	Price (IDR)			
		AFPMG		RFPMG	
		TPZ	RTG	CRV	RTG
1	Rotor	720,000	720,000	630,000	787,500
2	Stator	4,898,177	4,898,177	4,876,875	4,876,875
3	Magnet	8,037,362	7,385,684	8,254,588	7,385,684
4	Winding	609,675	609,675	634,050	634,050
		14,265,214	13,613,536	14,395,513	13,684,109

Table 7 describes that the AFPMG manufacturing cost, especially the RTG AFPMG offers the cheapest alternatives of per unit manufacturing cost. Another consideration in determining the best option for the machine topology is the cost per power unit. It is found that the RTG AFPMG has the lowest cost per unit of power ratio with IDR 20,178/watt and followed by CRV RFPMG, TPZ AFPMG, and RTG RFPMG with 23,292/watt, 24,028/watt, and 30,957/watt respectively.

6. Conclusion

The study has comprehensively compared generator performance and manufacturing cost across four distinct machine topologies: single gap AFPMG with rectangular and trapezoidal permanent magnet rotors and single gap inner rotor RFPMG with curved and rectangular permanent magnet rotors. Utilizing Ansys Maxwell 3D for finite element simulation, it was observed that the TPZ AFPMG exhibits the highest air gap flux density, whereas the RTG AFPMG generates the highest linkage flux due to its superior rotor pole-to-stator pole area ratio. Consequently, the RTG AFPMG demonstrates the highest output power and torque, while the RTG RFPMG performs the least favorably among the examined topologies. Furthermore, the RTG AFPMG exhibits the highest power-to-weight ratio, followed by the TPZ AFPMG, CRV RFPMG, and RTG RFPMG.

Manufacturing costs are determined using two approaches: multiplying the weight of active components by the manufacturing coefficient and considering the workshop price. Calculations reveal that the first method yields a lower manufacturing cost than the workshop price, making it more appropriate for mass production. Furthermore, neglecting shape variations, the first method consistently generates the same manufacturing cost when the magnet weight remains unchanged. On the other hand, the workshop price is better suited for creating a single prototype unit. Among the four machine topologies, it is evident that the RTG AFPMG exhibits the most cost-effective manufacturing, offering the lowest cost per unit of power. Conversely, RTG RFPMG stands out as the most expensive option.

Therefore, all findings support the conclusion that the axial flux type generator with rectangular magnets is the most profitable choice from a technical and economic standpoint.

Acknowledgements

The authors are grateful to the Research Centre for Energy Conversion Technology - National Research and Innovation Agency for all the facility support. We also thank the Ngombol Teknik workshop for the component manufacturing cost information.

Author Contributions

P.I. and K.W. were responsible for conceptualization, validation, resources, data curation, software development, and project administration. P.I., K.W., M. K. and P.W. jointly contributed to the methodology, formal analysis, investigation, original draft preparation, review and editing, visualization, and supervision. All authors have read and agreed to the published version of the manuscript.

Conflict of Interest

The author(s) declared no potential conflicts of interest with respect to the research, authorship, and/or publication of this article.

References

[1] R.S. Semken, M. Polikarpova, P. Röyttä, J. Alexandrova, J. Pyrhönen, and J. Nerg, "Direct-drive permanent magnet generators for high-power wind turbines: Benefits and limiting factors," IET Renewable Power Generation, vol. 6, pp. 1–8, 2012, doi: 10.1049/iet-rpg.2010.0191.

[2] K. Wirtayasa, P. Irasari, M. Kasim, P. Widiyanto, and M. Hikmawan, "Design of an axial-flux permanent-magnet generator (AFPMG) 1 kW, 220 V, 300 rpm, 1 phase for pico hydro power plants," in Proc. 2017 Int. Conf. on Sustainable Energy Engineering and Application, Jakarta, Indonesia, 23–24 Oct. 2017, pp. 172–179.

[3] V.B.M. Krishna, S.S.S.R.S. Duvvuri, K. Yadlapati, T. Pidikiti, and P. Sudheer, "Deployment and performance measurement of renewable energy based permanent magnet synchronous generator system," Measurement: Sensors, vol. 24, p. 100478, 2022, doi: 10.1016/j.measen.2022.100478.

[4] A. Belkaid, I. Colak, K. Kayisli, and R. Bayindir, "Modeling of a permanent magnet synchronous generator in a power wind generation system with an electrochemical energy storage," International Journal of Smart Grid, vol. 2, pp. 197–202, 2018.

[5] S. Vadi, F. B. Gürbüz, R. Bayindir, and E. Hossain, "Design and simulation of a grid connected wind turbine with permanent magnet synchronous generator," in Proc. 2020 8th Int. Conf. on Smart Grid (icSmartGrid), Paris, France, 17–19 June 2020, pp. 169–175.

[6] G. Landi, A. Musolino, L. Sani, and C. Simonelli, "Design criteria for an axial flux wind generator with Halbach array permanent magnets," in Proc. 12th Int. Conf. on Renewable Energy Research and Applications (ICRERA), Oshawa, Canada, 29 Aug.–1 Sept. 2023, pp. 213–218.

[7] S.S. Laxminarayan, M. Singh, A. H. Saifee, and A. Mittal, "Design, modeling and simulation of variable speed axial flux permanent magnet wind generator," Sustainable Energy Technologies and Assessments, vol. 19, pp. 114–124, 2017, doi: 10.1016/j.seta.2017.01.004.

[8] G. Ahmad and U. Amin, "Design, construction and study of small scale vertical axis wind turbine based on a magnetically levitated axial flux permanent magnet generator," Renewable Energy, vol. 101, pp. 286–292, 2017, doi: 10.1016/j.renene.2016.08.027.

[9] K. Latoufis, A. Matzakos, I. Katsambiris, A. Vassilakis, and N. Hatziargyriou, "Acoustic noise of axial flux permanent magnet generators in locally manufactured small wind turbines," IET Renewable Power Generation, vol. 13, pp. 2922–2928, 2019, doi: 10.1049/iet-rpg.2019.0164.

[10] W. Yao, M. Cheng, and J. Yu, "Novel design of a coreless axial-flux permanent-magnet generator with three-layer winding coil for small wind turbines," IET Renewable Power Generation, vol. 14, pp. 2924–2932, 2020, doi: 10.1049/iet-rpg.2019.0908.

[11] K. Wirtayasa and C. Hsia, "Performances comparison of axial-flux permanent-magnet generators for small-scale vertical-axis wind turbine," Alexandria Engineering Journal, vol. 61, pp. 1201–1215, 2020, doi: 10.1016/j.aej.2021.06.074.

[12] I. Topaloglu, Y. Nakanishi, F. Korkmaz, and Y. Nakashima, "Axial flux permanent magnet generator with low cogging torque for maintenance free under water power generating system," International Journal of Renewable Energy Research, vol. 6, pp. 510–519, 2016.

[13] T.S. El-Hasan, "Development of axial flux permanent magnet generator for direct driven micro wind turbine," in Proc. 2016 IEEE Int. Conf. on Renewable Energy Research and Applications (ICRERA), Birmingham, UK, 20–23 Nov. 2016, pp. 169–172.

[14] M. Vatani, A. Mohammadi, D. Lewis, J. F. Eastham, and D. M. Ionel, "Coreless axial flux Halbach array permanent magnet generator concept for direct-drive wind turbine," in Proc. 12th Int. Conf. on Renewable Energy Research and Applications (ICRERA), Oshawa, Canada, 29 Aug.–1 Sept. 2023, pp. 612–617.

[15] K. Latoufis, A. Konstantinidis, S. G. Fikari, and N. Hatziargyriou, "Comparison of coreless and soft magnetic composite core axial flux permanent magnet generators for locally manufactured pico-hydro plants," in Proc. 2018 IEEE Int. Conf. on Power Electronics, Drives and Energy Systems, Chennai, India, 18–21 Dec. 2018, pp. 1–6.

[16] V.D. Dio, G. Cipriani, and D. Manno, "Axial flux permanent magnet synchronous generators for pico hydropower application: A parametric study," Energies, vol. 15, pp. 1–17, 2022, doi: 10.3390/en15196893.

[17] H. Asiful and H. S. Che, "Design and simulation of axial flux permanent magnet generator for residential pico-hydro power generation," in Proc. Int. Conf. on Intelligent and Advanced System, Kuala Lumpur, Malaysia, 13–14 Aug. 2018, pp. 1–5.

[18] M.M. Ashraf, T. N. Malik, S. Zafar, and U. N. Raja, "Design and fabrication of radial flux permanent magnet generator for wind turbine applications," The Nucleus, vol. 50, pp. 173–181, 2013.

[19] A.R. Pramurti, E. Firmansyah, and Suharyanto, "Reduction on cogging torque in dual stator radial flux permanent magnet generator for low speed wind turbine," in Proc. 3rd Int. Conf. on Information Technology, Computer, and Electrical Engineering, Semarang, Indonesia, 19–20 Oct. 2016, pp. 1–4.

[20] R. Yazdanpanah, A. Afroozeh, and M. Eslami, "Analytical design of a radial-flux PM generator for direct-drive wind turbine renewable energy application," Energy Reports, vol. 8, pp. 3011–3017, 2022, doi: 10.1016/j.egyr.2022.01.121.

[21] H.Z. Agrebi, N. Benhadj, M. Chaieb, F. Sher, R. Amami, and R. Neji, "Integrated optimal design of permanent magnet synchronous generator for smart wind turbine using genetic algorithm," Energies, vol. 14, p. 4642, 2021, doi: 10.3390/en14154642.

[22] E.Y. Setyawan, Y. I. Nakhoda, A. U. Krismanto, L. Mustiadi, E. Yandri, and J. Burlakovs, "Design and construction of single phase radial flux permanent magnet generators for pico hydro scale power plants using propeller turbines in water pipes," in Proc. 4th Int. Conf. on Electrical Systems, Technology and Information, Bali, Indonesia, 24–27 Oct. 2019, pp. 1–20.

[23] E. Flores, M. Cumbajin, and P. Sanchez, "Design of a synchronous generator of permanent magnets of radial flux for a pico-hydropower station," in M. V. García, F. Peña, and C. G. Gallegos, Eds., Advances in Intelligent Systems and Computing, Singapore: Springer, 2021, pp. 135–151.

[24] P. Irasari, A. Muqorobin, P. Widiyanto, T. Nur, I. N. Diasta, and P. Sutikno, "Performance analyzes of a compact pico hydropower plant with a wide operating range," International Journal of Power Electronics and

Drive Systems, vol. 13, pp. 2357–2364, 2022, doi: 10.11591/ijpeds.v13.i4.pp2357-2364.

[25] G. Lee, H. Kim, T. Jung, and J. Kim, "Design study of dual generated radial flux permanent magnet generator for pico hydro generator," Applied Mechanics and Materials, vol. 212–213, pp. 1025–1029, 2012, doi: 10.4028/www.scientific.net/AMM.212-213.1025.

[26] O. Bouaziz, I. Jaafar, and F. Ammar, "Performance analysis of radial and axial flux PMSM based on 3D FEM modeling," Turkish Journal of Electrical Engineering & Computer Sciences, vol. 26, pp. 1587–1598, 2018, doi: 10.3906/elk-1708-68.

[27] S. Bhuvaneswari, P. Sivaraman, A. Matheswaran, and P. Prem, "Performance analysis of radial flux and axial flux permanent magnet generators for low-speed wind turbine applications," International Journal of Applied Electromagnetics and Mechanics, vol. 1, pp. 1–19, 2020, doi: 10.3233/JAE-190150.

[28] Y. Park, M. Koo, S. Jang, J. Choi, and D. You, "Performance evaluation of radial- and axial-flux PM wind power generators with mechanical energy storage system," IEEE Transactions on Energy Conversion, vol. 30, pp. 237–245, 2015, doi: 10.1109/TEC.2014.2331246.

[29] A.A. Pop, F. Jurca, C. Oprea, M. Chirca, and S. Breban, "Axial-flux vs. radial-flux permanent-magnet synchronous generators for micro-wind turbine application," in Proc. 2013 15th European Conf. on Power Electronics and Applications, Lille, France, 2–6 Sept. 2013.

[30] M. Chirca, S. Breban, C. Oprea, and M. M. Radulescu, "Comparative design analysis of ferrite-permanent-magnet micro-wind turbine generators," in Proc. 2015 Int. Aegean Conf. on Electrical Machines & Power Electronics, Side, Turkey, 2–4 Sept. 2015, pp. 1–10.

[31] M.R. Dubois and H. P. J. A. Ferreira, "Axial and radial-flux PM generators for direct-drive wind turbines," in Proc. European Wind Energy Conf. and Exhibition, Copenhagen, Denmark, 2–6 July 2001, pp. 5–8.

[32] F. Meier and J. Soulard, "PMSMs with non-overlapping concentrated windings: Design guidelines and model references," in Proc. Ecologic Vehicles and Renewable Energies, Monaco, 26–29 Mar. 2009, pp. 1–9.

[33] A.M. El-Refaie, M. R. Shah, J. P. Alexander, S. Galioto, K. Huh, and W. D. Gerstler, "Rotor end losses in multiphase fractional-slot concentrated-winding permanent magnet synchronous machines," IEEE Transactions on Industry Applications, vol. 47, pp. 2066–2074, 2011, doi: 10.1109/TIA.2011.2162049.

[34] D. Gerling, Electrical Machines: Mathematical Fundamentals of Machine Topologies, Berlin, Germany: Springer, 2015.

[35] F. Sahin, "Design and development of a high-speed axial-flux permanent machine," Ph.D. dissertation, Eindhoven University of Technology, Eindhoven, The Netherlands, 2001.

[36] J. Zhao, B. Li, and Z. Gu, "Research on an axial flux PMSM with radially sliding permanent magnets," Energies, vol. 8, pp. 1663–1684, 2015, doi: 10.3390/en8031663.

[37] Strategic Metals Invest, "Neodymium prices," 2023. [Online]. Available: https://strategicmetalsinvest.com/neodymium-prices/ [Accessed: Dec. 13, 2023].